



Ferricrete biochemical degradation on the rainforest–savannas boundary of Central African Republic

Anicet Beauvais

► To cite this version:

Anicet Beauvais. Ferricrete biochemical degradation on the rainforest–savannas boundary of Central African Republic. *Geoderma*, 2009, 150, pp.379-388. 10.1016/j.geoderma.2009.02.023 . hal-01097326

HAL Id: hal-01097326

<https://hal.science/hal-01097326>

Submitted on 23 Dec 2016

HAL is a multi-disciplinary open access archive for the deposit and dissemination of scientific research documents, whether they are published or not. The documents may come from teaching and research institutions in France or abroad, or from public or private research centers.

L'archive ouverte pluridisciplinaire **HAL**, est destinée au dépôt et à la diffusion de documents scientifiques de niveau recherche, publiés ou non, émanant des établissements d'enseignement et de recherche français ou étrangers, des laboratoires publics ou privés.

Ferricrete biochemical degradation on the rainforest-savannas

boundary of Central African Republic

Anicet Beauvais

CEREGE (Centre Européen de Recherche et d'Enseignement des Géosciences de

l'Environnement), Aix-Marseille Université, CNRS, INSU, IRD, CdF, Europôle

Méditerranéen de l'Arbois, BP 80, 13545 Aix-en-Provence Cedex 4 France

beauvais@cerege.fr (tel./fax: (33) 4 42 97 17 73/4 42 97 15 95)

Abstract

In southeastern Central African Republic the lateritic weathering mantles are capped by two to five meters thick ferricretes, which previously formed under a seasonal tropical climate. The actual humid tropical climatic conditions result in the biophysical disaggregation of the ferricretes everywhere the forest develop that lead to a soil formation composed of ferricrete relicts and ferruginous nodules embedded in a soft bioturbated micro-aggregated clay-ferruginous matrix. The potential effect of the biological activity (e.g., termites) on the soil and vegetation dynamics and therefore on the evolution of the previous consolidated ferricrete is discussed. Following its mechanical disaggregation by the forest tree roots, the ferricrete underwent a chemical degradation under the combined effect of hydration and redox conditions, which result from the biodegradation and oxidation of the organic matter. The transformation of the ferricrete into a soft bioturbated micro-aggregated clay-ferruginous soil matrix implies the hematite dissolution, and the kaolinite transformation into gibbsite, which may characterize a late “bauxitization” (secondary gibbsitization of kaolinite) of previous ferricrete profiles linked to a late Quaternary environmental (climate and vegetation) change. However, the geochemical and mineralogical pattern of the matrix not only reflects the geochemistry of the parental ferricrete but also depends on the physical transfers of quartz and heavy minerals from the lower horizons of the profile. Hence, the use of geochemical indexes such as Ti and/or Zr for mass balance calculations in the lateritic weathering profiles is precluded because these supposedly inert chemical elements are not simply accumulated by *in situ* chemical weathering process.

Keywords: Biochemical weathering; Ferricrete; Bauxitization; Termites; Central African Republic

Beauvais, 2008

1. Introduction

Long term rock chemical weathering throughout the intertropical zone led to the formation of several tens meters of lateritic weathering profiles, many being capped by two to ten meters thick ferricretes. From the bottom to the top, a ferruginous lateritic weathering profile is generally composed of a saprolite, a mottled clay horizon, a soft ferricrete and/or a soft nodular horizon and a ferricrete (Nahon, 1986; Tardy, 1997; Beauvais, 1999). The ferricretes developed under a seasonal tropical climate and represent the ultimate stage of the ferruginization process that started earlier in the mottled clay horizon (Tardy and Nahon, 1985; Nahon, 1986, 1991; Thomas, 1994; Tardy, 1997; Beauvais, 1999). With the increasing ferruginization, the geochemical signature of parent rocks is progressively blurred until nearly complete deletion in the ferricrete (Tardy et al., 1988; Tardy, 1997). The large intertropical areas over which the ferricretes actually outcrop suggest paleoclimatic changes towards drier conditions (Tardy and Roquin, 1998) that led to the degradation of the vegetation cover with a consecutive mechanical erosion of the upper leached horizon, which previously overlay the buried ferricrete (Büdel, 1982; Millot, 1983; Butt, 1987).

However, the exposed ferricretes may disaggregate and geochemically degrade under the wet and warm climatic conditions characterizing the rainforest environments (Novikoff, 1974; Nahon *et al.*, 1989; Thomas, 1994; Tardy, 1997). The degradation of previously consolidated ferricretes implies a complete reorganization of the uppermost part of the profile under the effects of biological activity and almost permanent moisture. Therefore, the disaggregated ferricrete is progressively transformed into a soil containing blocks and debris of ferricrete of various sizes including centimeter size ferruginous nodules embedded in a bioturbated micro-aggregated clay ferruginous matrix similar to that of many red ferruginous tropical soils. Such a transformation is

investigated (1) by comparing the main geochemical outlines of an undisturbed ferricrete profile and a disaggregated ferricrete horizon, and (2) by defining the geochemical differentiation pattern of two disaggregated ferricrete horizons at the top of lateritic weathering profiles profile developed upon different parent rocks. The biophysical and geochemical processes involved in the ferricrete degradation are discussed. In particular, the potential role of the biological activity (e.g., termites) on the degradation processes of previous undisturbed ferricrete profiles is approached.

2. Field description

The study area (“Haut Mbomou”) is located in southeastern Central African Republic (CAR) (Fig. 1a). The climate is humid seasonal tropical with a dry season from December to February and a mean annual rainfall of 1600 mm (Fig. 1a), a mean annual temperature of 25°C and a mean annual relative humidity of the air of 80%. The southern part of CAR hosts forests belonging to the Congo-Guinean domain (Sillans, 1958), where *Terminalia superba*, *Albizia zygia*, *Triplochiton scleroxylon* and *Celtis sp.* are the main identified species (Boulvert, 1986; Beauvais, 1991).

The vegetation of the study area is a mosaic of grass savanna interspersed with patches of dense rain forest. About 79.3 % of the total landsurface of the previous mapped area (545 km²) are covered by grass savanna where consolidated ferricrete is outcropping on plateaus and hillslopes, while the rain forest occupies the remaining 20.7 % where the ferricrete is disaggregated resulting in the formation of dismantled ferricrete soils (Beauvais and Roquin, 1996; Fig. 1b). The extension of forest against savanna in the Mbomou area was dated from the Holocene period using C isotopic analyses of organic matter in soils and alluvial sediments (Runge, 2002) that also characterize a climatic change towards more humidity. A semi-humid forest with

Beauvais, 2008

Anogeissus leiocarpus and *Albizia zygia* effectively develops around the highest plateaus (10.6% of the total surface) at a topographic slope gradient change (Fig. 1c), while a Guinean selva forest with *Triplochiton scleroxylon* and *Celtis sp.* occupies relatively incised thalwegs (10.1% of the total surface). A Soudano-Guinean savanna with *Daniella oliveri* and *Terminalia glaucescens* alternates with Gramineae such as *Ctenium newtonii* and *Loudetia annua* (Sillans, 1958), where ferricrete effectively outcrops on the plateaus (Boulvert, 1986; Beauvais, 1991).

The degradation processes of the ferricrete are investigated on vertical profiles located in the forested transition area between the high plateaus and the bare hillslope (Figs. 1b and 1c), which carry massive or protonodular and protopisolitic ferricretes, respectively, as previously established from a combined geomorphological and petrological study of the main ferricretes in the “Haut-Mbomou” region (Beauvais and Roquin, 1996). In the “Haut-Mbomou” area, the moderate epeirogenesis resulted in insufficient river incision and erosion that did not allow a clear differentiation of stepped lateritic paleolandscapes (bauxitic and ferruginous) like those characterizing the West African landscapes (Eschenbrenner and Grandin, 1970, Michel, 1973; Grandin, 1976; see also Beauvais et al., 1999). The long-term (Cenozoic) climatic change gradient was higher in West Africa than in CAR (Tardy and Roquin, 1998). Paleoclimates evolved from humid to dry in West Africa, and from arid to seasonal humid tropical in CAR that led to continuous ferricrete formation during Tertiary (Beauvais, 1991; Beauvais and Colin, 1993; Tardy and Roquin, 1998) instead of successive development of bauxite and ferruginous glaciais (pediments). However, the high plateaus and hillslopes or low plateaus of the “Haut-Mbomou” could be analogous of the West African intermediary and high glaciais landscapes, respectively (Boulvert, 1996).

The “Haut-Mbomou” landscape is also characterized by “mushroom” termite mounds of *Cubitermes fungifaber*, which are systematically erected on gently sloping surfaces bearing a ferricrete (Fig. 3a), called “lakéré” (Sillans, 1958; Boulvert, 1986). Runge and Lammers (2001) counted five to six hundred termite mounds per hectare for an area of 75,000 km² (Mbomou plateau) that imply a denudation rate of 0.1 mm.ha⁻¹.year⁻¹ corresponding to 0.94 t. ha⁻¹.year⁻¹ of material removed by termites from the lower weathered horizons (saprolite and mottled clays). This material is therefore available for surface runoff erosion and dispersion over the outcropping ferricretes (Fig. 3b) that may favor the forest growth at the expenses of savanna under humid tropical climatic conditions.

3. Material and analytical techniques

The degradation patterns of the ferricrete are studied and analyzed in the uppermost-disaggregated parts (1 to 4.5 m) of two vertical lateritic weathering profiles (Figs. 2c and 2d) at Guenekoumba and Finzani in southeastern CAR (Figs. 1a). The two vertical profiles are located in the forest fringe (forested hillslope) between the high plateau and the bare hillslope both bearing undisturbed ferricrete profiles (Fig. 1b). The weathering profile of Guenekoumba is developed on amphibole schist (Beauvais and Colin, 1993) while epimetamorphic schist intruded by granite constitutes the parent rocks of the Finzani weathering profile. Based on geological map, the amphibole schist rocks were observed and collected on outcrops and in riverbeds, while the epimetamorphic schist was deduced by the direct observation of saprolites (Beauvais, 1991; Beauvais and Colin, 1993). A typical disaggregated ferricrete horizon is composed of three main components (Fig. 2b to 2d). A first component corresponds to the disaggregated ferricrete of 1-2 to 3 m thickness, which is often affected by

horizontal joints (Fig. 2c and 2d), the edges of which being overlain by lamellar goethitic brown secondary deposits. Decimetric and metric fragments and blocks of ferricrete characterize this sub-horizon. The second component is composed of hematitic ferruginous nodules and clasts of ferricrete of size ranging between 1 and 10 cm. This sub-horizon can also contain some humus in its uppermost part. The nodules are larger at the top than at the base of the horizon. The third component consists of the bioturbated micro-aggregated clay-ferruginous matrix, in which the nodules and clasts of ferricrete are embedded and the biological activity is highly developed (Fig. 2b).

Fifty-three samples and sub-samples were collected between 0 and 4.5 meters (Figs. 2c and 2d): thirty-three samples for Guenekoumba (15 ferricrete relicts, 9 nodules and 9 matrices) and twenty samples for Finzani (6 ferricrete relicts, 6 nodules and 7 matrices). Subsamples of nodules and matrices were extracted from a same sample.

XRD was used to determine the mineral composition of each sample category, i.e., the quantity of quartz, kaolinite, gibbsite, hematite and goethite. Mineral contents were estimated by measuring characteristic intensity of X-ray peak weighted by a calibration coefficient defined for each mineral, using normative calculations (Mazaltarim, 1989). The estimation error ranges from 1 to 3 %. Each sample was therefore defined by five mineralogical variables, corresponding to the estimated contents of kaolinite (Ka), quartz (Q), gibbsite (Gi), goethite (Go), hematite (He), and also by the ratios, R_{GH} equal to $100 * \text{goethite} / (\text{goethite} + \text{hematite})$, and R_{KGi} equal to $100 * \text{kaolinite} / (\text{gibbsite} + \text{kaolinite})$ as defined by Beauvais and Roquin (1996). Scanning electron microscopy has been also used to define the crystalline morphology of the main mineral phases for each ferricrete degradation component.

Spark emission spectrometry has provided chemical composition for major elements, Si, Al, Fe, Mn, Mg, K, Ti, P. Inductively coupled plasma atomic emission

spectrometry (ICP-AES) was used to dose the trace elements, Sr, Ba, V, Ni, Co, Cr, Zn, Cu, Sc, Y, Zr, La, Ce, Yb, Nb.

Mineralogical and chemical data were statistically analyzed by a principal component analysis (PCA) using StatView F- 4.5 (1995) that allowed differentiation of the main geochemical patterns of each sample category. The eigenvectors are first determined with their associated Eigen values from the correlation matrix, followed here by an application of the orthogonal Varimax rotation procedure (Lebart *et al.*, 1979). The principal components (factorial axes) describe the main differentiation trends in the data set. These independent synthetic variables are characterized by correlation loadings with chemical elements and minerals, as previously applied to tropical soils (Litaor *et al.*, 1989; Donkin and Fey, 1991), bauxitic weathering profiles and ferricretes regional distribution (Boski and Herbosch, 1990; Roquin *et al.*, 1990; Beauvais and Roquin, 1996). Within each factor, the correlation loadings ranging from -0.4 to 0.4 were considered as non-significant regarding to the samples number. The projection of samples on factor score diagrams highlights the differentiation patterns within and between each samples category, allowing discussion of the geochemical and mineralogical evolution induced by the development of the weathering and ferruginization and/or the ferricrete degradation process.

4. Results and discussion

4.1. Petrographical outlines of the ferricrete degradation

The formation processes of undisturbed lateritic weathering profiles (Fig. 2a) were previously studied (Beauvais and Colin, 1993; Beauvais, 1999). The present study focuses on the uppermost part (ferricrete) of such profiles, which is apparently disaggregated and degraded under the forest (Fig. 2b). The ferruginous nodules of such

horizon have the same petrographical fabric as the ferricrete. However, many nodules exhibit peripheral goethite brown rims (Fig. 4a) composed of many thin crystals, which develop perpendicular to the edge of the hematitic core of the nodules (Fig. 4b). Other nodules previously composed of hematite and kaolinite (Beauvais, 1999) show gibbsite crystals formed at the expense of the kaolinite (Fig. 5a). Secondary gibbsite crystals of 10 μm size are also observed within vacuolar voids of 20 to 50 μm sizes (Fig. 5b). The bioturbated micro-aggregated clay ferruginous matrix is also characterized by the formation of smaller size (2 μm) gibbsite crystals within the vacuolar and tubular porosity (Fig. 6a and 6b). This gibbsite is not inherited but comes from the process of ferricrete transformation, contemporaneously with the secondary gibbsite forming in the kaolinitic saprolite of undisturbed profiles (Beauvais and Colin, 1993; Beauvais, 1999). The degradation matrix also contains small size (10 μm) quartz grains (Fig. 6c and 6d), which may be mechanically transferred from other parts of the profile through the termite activity (Eschenbrenner, 1986; Tardy, 1997; Thomas, 1994).

4.2. Undisturbed versus disaggregated ferricrete profile

A comparison between a previously studied undisturbed lateritic weathering profile with consolidated ferricrete (Beauvais and Colin, 1993) and the disaggregated ferricrete horizon of an adjacent profile in the Guenekoumba site (Figs. 2a, 2b and 2c) allows differentiation between the advancing ferruginization and the geochemical degradation of ferricretes. The development of the undisturbed weathering profile is a function of two complementary processes: saprolitization and ferruginization (Beauvais and Colin, 1993), during which iron first increases by relative accumulation (saprolitization) and secondly by absolute accumulation that leads to the ferricrete development (Beauvais, 1999). These processes are characterized by analyzing the behavior of Fe against Sc (Brown et al., 2003). Except for the

absolute Fe depletion due to local reduction process in the saprolite, Fe and Sc increase in same proportions (relative Fe accumulation) during the first stage of *in situ* rock chemical weathering. However, Fe and Sc show a more contrasted behavior during the ferruginization process driven by oxidation processes that lead to the development of the soft nodular and ferricrete horizons by absolute Fe accumulation (Fig. 7a).

The ferricrete geochemical degradation first leads to a decrease of Sc compared to the ferricrete of the undisturbed profile, then to a decrease of Fe with approximately constant Sc (Fig. 7a). The nodules of the disaggregated horizon are richer in Fe than the nodules of the soft nodular layer underlying the ferricrete of the undisturbed profile. The first effectively derive from the physical disaggregation and geochemical degradation of the ferricrete, whereas the second are advanced ferruginized forms of mottled clays (Tardy and Nahon, 1985; Nahon, 1986, 1991; Tardy, 1997). The matrices of the disaggregated ferricrete horizon show less Sc content than the saprolite and the mottled clays of the undisturbed ferricrete profile (Fig. 7a). These matrices are also enriched in Zr and Si (Quartz), and show similar Ti contents as the saprolite and mottled clays of the undisturbed ferricrete profile (Figs. 7b-d). Ti and Zr are not correlated in the undisturbed profile while they co-vary in the disaggregated ferricrete horizon (Fig. 7d). They may relatively enrich from the ferricrete degradation or absolutely accumulate by some mechanical transfer from other parts of the profile.

A principal component analysis of the geochemical and mineralogical data of the undisturbed and disaggregated profiles yields four factorial axes describing 75.2% of the total variance (Table 1). The first factorial axis (37.3 % of the total variance) discriminates the saprolitization with its residual parent rock mineralogical inheritance (quartz + heavy minerals) from the advancing ferruginization (hematite and goethite) processes (Fig. 8). The second factorial axis (23.6 % of the total variance) characterizes

the ferricrete degradation by discriminating the clay-ferruginous matrices from the ferricrete relicts and nodules (Fig. 8). The figure 8 also shows the differentiation of the degradation matrices from the saprolite and mottled clays of the undisturbed ferricrete profile. Compared to the parental ferricretes the degradation matrices are enriched in quartz, gibbsite and heavy minerals and impoverished in iron, hematite and kaolinite. The third factorial axis (7.2 % of the total variance) clearly described the transformation of kaolinite into gibbsite in the undisturbed ferricrete profile (Beauvais and Colin, 1993) but also in the degradation matrices (Table 1 and Figs. 6a-b) that could characterize the late “bauxitization” (i.e., secondary gibbsitization according to Tardy, 1997) of the previous ferricrete profiles. This “bauxitization” may result from the development of the forest at the expenses of savanna linked to a more humid climate since the Holocene (7.5 to 7 ka) (Runge, 2002). The fourth factorial axis (7.1 % of the total variance) collates Ce, Ba, Sr and La, which reflect some parent rock geochemical inheritance (Table 1). Secondary minerals such as florencite may also form as it was suggested in similar lateritic weathering profiles of Cameroon (Braun et al., 1990). Cerianite (Ce-oxide) was also identified at the bottom of the soft nodular horizon in the undisturbed ferricrete profile of Guenekoumba (Beauvais and Colin, 1993).

4.3. Geochemical differentiation pattern of two disaggregated ferricrete horizons

The average geochemical and mineralogical compositions of each ferricrete degradation components (ferricrete elements, nodules and soft matrices) are given in the table 2. The degradation components of the Guenekoumba profile are, on the average, less rich in silica, alumina, MgO, and K₂O but richer in Fe₂O₃, Mn₃O₄, TiO₂ and P₂O₅ than those of the Finzani profile. These geochemical differences reflect differences of parent rocks, which are also emphasized by differences in V, Cr, Cu, Zn, Y, Ba, La and

Ce contents (Table 2). A relatively high amount of K₂O and Ba has been noted in the Finzani ferricrete relicts as well as some Mg (Table 2) that may indicate a relatively quick ferruginization of saprolite still embedding poorly weathered micas prior to the hardening of the ferricrete (Beauvais, 1991, 1999). Therefore, the differences of alumina contents may be explained by the accumulation of relict micas and kaolinite higher in the Finzani profile than in the Guenekoumba profile (Table 2).

The geochemical differentiation patterns of each sample category (ferricrete relicts, nodules, and matrix) are also deciphered, by applying a Principal Component Analysis (PCA) to the geochemical and mineralogical data that allows definition of three factorial axes accounting for 76.4 % of the total variance (Table. 3). The first factorial axis (44.1 % of the total variance) discriminates the group (ferricrete relicts + the ferruginous nodules) from the embedding clay-ferruginous matrices (Fig. 9). These latter are enriched in quartz (Figs. 6c-d and 10a) and heavy minerals (Fig. 10b) and they are propitious to the development of gibbsite (Figs. 6a-b and 11a), which results from the late weathering of micas and/or from the desilification and hydration of kaolinite (Beauvais and Roquin, 1996). With quartz, the heavy minerals compose the residual mineral phase, which may be relatively enriched by *in situ* geochemical degradation of ferricrete containing them (Figs. 9 and 10b) or mechanically transferred with the clay-silt materials from other parts of the profile through the termite activity (Tardy and Roquin, 1992). The variation of Zr content in matrices at constant Fe (Fig. 11b) may also suggest, at least partially, an absolute input of small size zircon. Hence, the common use of Ti and Zr for mass balance calculations should be considered with much caution. Zircon may also dissolve in the lateritic geosphere (Colin *et al.*, 1993). Mass balance calculations based on geochemical indexes may be applied for non-perturbed weathering horizons (Beauvais and Colin, 1993) but they are inappropriate for

quantifying the geochemical mass balance transfers in the upper ferruginous horizons that are bioturbated and often rework allochthonous materials (Beauvais et al., 1999).

The geochemical degradation of the ferricrete therefore leads to a release of Fe_2O_3 , Sr, Ba, V, and Cr, with an accumulation of silica, alumina, Mn_3O_4 , MgO, K_2O and TiO_2 in the matrices, and also, Ni, Y, Zr, Yb and Nb. The amounts of P_2O_5 , and Co, Zn, Cu, Sc, La, and Ce remain relatively constant (Table 2). The increasing of magnesium and potassium in the matrices of degradation profiles may reflect the occurrence of poorly weathered micas as phengites that is indicated by the negative loading of the second factorial axis (20.9 % of the total variance). Previous geochemical analyses of saprolite and mottled clays of Guenekoumba undisturbed profile revealed similar Mg and K contents, which related to poorly weathered relict micas optically identified on thin sections (Beauvais and Colin, 1993). The second factorial axis also characterizes the association of goethite with Cu, TiO_2 , Zn, P_2O_5 , Mn_3O_4 , and Sc (Table 3), which may indicate the presence of anatase and/or residual ilmenite in the degradation matrices as previously shown in undisturbed weathering profile (Beauvais and Colin, 1993). The factor 2 therefore discriminates the Ti-rich Guenekoumba degradation profile from the Ba-Mg-K rich Finzani degradation profile (Fig. 9) that suggests incomplete micas dissolution in this profile although a part of the kaolinite may derive from their late weathering in the degradation matrices (Table 2). The third factorial axis (11.4 % of the total variance) discriminates La–Sr–Ce–V from Co–Cu–Sc–Ni that reflects some geochemical dependence to the parent rock.

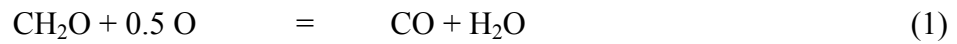
4.4. Factors of the ferricrete biochemical degradation

The mechanical disaggregation (tree roots effect) and biochemical degradation of the ferricrete result in the loosening of the ferruginous cements and their bioturbation by

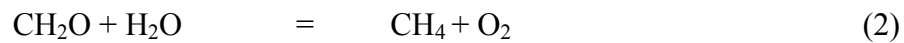
burrowing animals such as worms and termites. Termites microdivide the mineralogical assemblages and transfer nutrients and clay-silts from the saprolite to the upper ferruginous horizons and the topsoils (Eschenbrenner, 1986, 1987; Gleeson and Poulin, 1989; Tardy and Roquin, 1992; Thomas, 1994). Many topsoils of Central Africa are formed, at least in part, from imported material from deeper horizons by termite activity (De Heinzelin, 1955; De Ploey, 1964). The termite material may be spread at the ground surface by erosion (Fig. 3b) that effectively contributed to the soil restoration and hillslope forestation (Mando et al., 1996; Runge and Lammers, 2001), which are further sustained by the nutrients transferred from the bottom to the top of the profiles (Miedema et al., 1994; Berner and Berner, 1996). The forest biochemically degrades the ferricrete transforming its main mineralogical constituents (Tardy and Roquin, 1992; Birkeland, 1999). Notice that many ferruginous “stone lines” of the tropical forest savanna transition areas may result from the combined termite activity and ferricrete biophysical degradation (Eschenbrenner, 1986, 1987).

In spite of the lack of specific biogeochemical data, some interesting idea based on field observations may be discussed before to be tested in future investigations. The increasing biological activity generates bioturbation and aeration of the lateritic weathering profiles by creating channels, chambers and pedotubules that improve the hydrological properties of soils (drainage) and the plants development (Humphreys, 1994; Mando et al., 1996; Runge and Lammers, 2001). The digestion of the organic matter by termites modifies the redox conditions of the vadoze zone. In the lateritic profiles evolving under a forest cover the organic matter biodegradation may result in a degassing of a mixture of carbon monoxide and methane. The occurrences of degassing and water at the bottom of 10 to 15 m thick profiles may have a biogeochemical impact on the geochemical and mineralogical patterns of the lateritic weathering profiles.

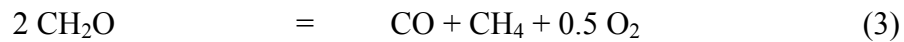
Although the gases were not analytically identified, they were highly suspected by acid smells owing to the organic matters decomposition, by experimenting burn rope (CO) and observing termite activity (CH₄) at the transition between the saturated and unsaturated zone of profiles (10 to 15 meter depth). Carbon monoxide derives from the partial oxidation of organic matter as:



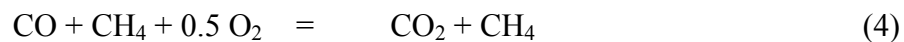
Methane result from the biodegradation of organic matter in termites' guts (Berner and Berner, 1996; Mackenzie, 1998) according to the following reaction:



It results from (1) and (2) the global dissociation reaction of organic matter:



That leads to carbon dioxide production with methane as:



It would be certainly interesting to analytically characterize the organic species in the degradation matrices and in the solutions draining the disaggregated ferricrete profiles as well as to get C isotopic signatures of the organic matters, soil solutions, and gaseous phases. For instance, the measure of ¹³C/¹²C ratios would be useful to

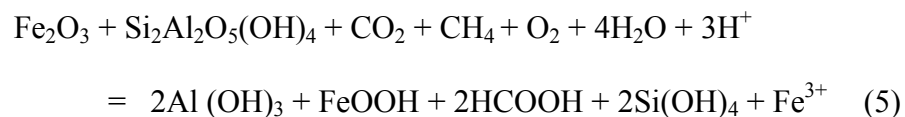
distinguish bacterial from non-bacterial sources of methane (Conny and Currie, 1996).

However, the geochemical degradation of the ferricrete including the transformation of its mineralogical constituents may be primarily controlled by the degree of hydration of the profile (Tardy, 1997), and by the redox conditions change owing to the biodegradation of organic matters producing H^+ protons (Berner and Berner, 1996).

4.5. Mineralogical outcomes of the ferricrete biochemical degradation

The increasing biological dynamics and soil moisture (pore water activity) therefore result in an increase of gibbsite and in a lesser part goethite with respect to kaolinite and hematite. Goethite content does not significantly increase (Table. 1), but hematite is partly dissolved under the combined effect of redox and hydration process.

The organic matter biodegradation (reaction 4) and hydration processes may effectively create the conditions of the disruption of the hematite – kaolinite mineral association according to the following reaction:



The released Fe may be exported towards the lower parts of the profiles and reincorporated in a newly formed ferricrete essentially composed of goethite (Beauvais, 1999), according to local redox conditions also favorable to the formation of Ce and Mn-oxhydroxydes (Beauvais and Colin, 1993).

The matrices and ferruginous nodules of the Guenekoumba profile are a little more gibbsitic but less kaolinitic than those of the Finzani profile (Figs. 10a and 11a).

Nodules and ferricretes of Finzani contain more kaolinite than those of Guenekoumba

(Fig. 11a) but the same gibbsite quantities. According to Tardy (1997), the transformation of kaolinite into gibbsite is limited in quartz-rich matrices, while this transformation is important in matrices impoverished in quartz. But our results show that relatively high quantities of small size quartz in bioturbated matrices (Figs. 6c-d and 10a) do not preclude the transformation of kaolinite into gibbsite (Figs. 6a-b and 11a). In tropical soils this transformation is driven by high water activity ($[H_2O] = 1$) in large pores (Tardy, 1997). Gibbsite effectively derives from kaolinite according to desilification and hydration processes that lead to a decrease of kaolinite in the matrices compared with the contents measured in the ferricrete and nodules (Fig. 11a). However in soils with similar physical chemical properties (porosity, water activity and Eh-pH conditions), the presence of silicates as phengites and quartz maintains relatively high amounts of Si, Al, and (Ba, K, Mg) within the matrices (Table 2) that may limit the transformation of kaolinite into gibbsite (Fig. 10a). This is the case of matrices of the Finzani degradation profile (Fig. 11a) where the quantity of poorly weathered micas inherited from the deeper horizons is higher than in the Guenekoumba profile. Therefore, a part of the kaolinite may derive from the late weathering of micas if the water activity in matrix pores is ≤ 0.9 ; but hematite could remain stable (Trolard and Tardy, 1987). However, it was previously shown that kaolinite deriving from micas is large and well crystallized and could be a mineralogical tracer of the late ferricrete degradation (Beauvais and Bertaux, 2002). Both micas and kaolinite may however transform into gibbsite if the water activity > 0.9 (Tardy, 1997), and the hematite is dissolved and partly transformed into goethite (Trolard and Tardy, 1987).

5. Conclusion

In transitional humid tropical environments between savanna and rainforest, the degradation of ferricrete previously composed of hematite and kaolinite results in the development of a softer material relatively richer in gibbsite and in a lesser part in goethite. The ferricrete degradation horizon is composed of chemically unsaturated ferricrete relicts and ferruginous nodules embedded in a bioturbated micro-aggregated clay ferruginous matrix. This matrix is also enriched in poorly weathered parent minerals such as micas inherited from lower saprolite, and also with small size quartz and heavy minerals, which may be biomechanically transferred by termites from the lower horizons of the lateritic weathering profiles. The nutrient supplies by termites may sustain the forest recrudescence on previous savanna areas implying the biophysical dismantling and the geochemical degradation of the ferricrete. Such an ecosystem may self-organize according to a positive feedback loop in that, the more humid becomes the climate, the faster the forest grows in area enriched in nutrients imported by termites, the more the ferricrete transforms into a micro-aggregated soil, which sustains the forest development and therefore its destructive effect on the ferricrete. The resulting hydration and biological processes lead to the biodegradation and oxidation of organic matters modifying the redox conditions that also trigger the ferricrete degradation. These processes result in the preferential dissolution of hematite, and the transformation of kaolinite into gibbsite provide the moisture (water activity) be sufficient that may also characterize the late “bauxitization” (Holocene) of previous ferricrete profiles.

Acknowledgements – This is an IRD (UMR 161 CEREGE) contribution, which was previously supported by the research program PIRAT (INSU-CNRS-ORSTOM). Two anonymous reviewers are thanked for their helpful remarks and suggestions.

References

- Beauvais, A., 1991. Paléoclimats et dynamique d'un paysage cuirassé du Centrafrique. Morphologie, Pétrologie et Géochimie. Ph. D. Thesis, University of Poitiers, France.
- Beauvais, A., 1999. Geochemical balance of lateritization processes and climatic signatures in weathering profiles overlain by ferricrete in Central Africa. *Geochim. Cosmochim. Acta* 63, (23/24), 3939-3957.
- Beauvais, A., Bertaux, J., 2002. In situ characterization and differentiation of kaolinites in lateritic weathering profiles using infrared microspectroscopy. *Clays Clay Miner.* 50/3, 314-330.
- Beauvais, A., Colin, F., 1993. Formation and transformation processes of iron duricrust systems in tropical humid environment. *Chem. Geol.* 106, 77-151.
- Beauvais, A., Ritz, M., Parisot, J-C., Dukhan, M., Bantimimba, C., 1999. Analysis of poorly stratified lateritic terrains overlying a granitic bedrock in West Africa, using 2-D electrical resistivity tomography. *Earth Planet. Sci. Letters* 173, 413-424.
- Beauvais, A., Roquin, C., 1996. Petrological differentiation patterns and geomorphic distribution of ferricretes in Central Africa. *Geoderma* 73, 63-82.
- Berner, E. K., Berner, R. A., 1996. Global environment, Water, Air, and Geochemical Cycles. Prentice Hall.
- Birkeland, P.W., 1999. Soils and Geomorphology. Oxford University Press, New York.
- Boski, T., Herbosch, A., 1990. Trace elements and their relation to the mineral phases in the lateritic bauxites from southeast Guinea-Bissau. *Chem. Geol.* 82, 279-297.
- Boulvert, Y., 1986. Carte phytogéographique de la République Centrafricaine à 1: 1.000.000. feuille Ouest, feuille Est. ORSTOM, collection notice explicative, 104, Paris.
- Boulvert, Y., 1996. Etude géomorphologique de la République Centrafricaine. Notice explicative de la carte à 1/1 000 000. ORSTOM, Paris.

- 498 Braun, J.-J., Pagel, M., Muller, J.-P., Bilong, P., Michard, A., Guillet, B., 1990. Cerium
 499 anomalies in lateritic profiles. *Geochim. Cosmochim. Acta* 54, 781-795.
- 500 Brimhall, G. H., Lewis, C. J., Ford, C., Bratt, J., Taylor, G., Warin, O., 1991. Quantitative
 501 geochemical approach to pedogenesis: importance of parent material reduction, volumetric
 502 expansion, and eolian influx in lateritization. *Geoderma* 51, 1-4, 51-91.
- 503 Brown, D. J., Helmke, P. A., Clayton, M. K., 2003. Robust geochemical indices for redox and
 504 weathering on a granitic laterite landscape in Central Uganda. *Geochim. Cosmochim. Acta*
 505 67, 2711-2723.
- 506 Büdel, J., 1982. Climatic geomorphology. Princeton University Press, Princeton, New
 507 Jersey.
- 508 Butt, C.R.M., 1987. A basis for geochemical exploration models for tropical terrains.
 509 *Chem. Geol.* 60, 5-16.
- 510 Colin, F., Alarcon, C., Vieillard, P., 1993. Zircon: an immobile index in soils ? *Chem. Geol.*
 511 107, 273-276.
- 512 Conny, J. M., Currie, L. A., 1996. The isotopic characterization of methane, non-methane
 513 hydrocarbons and formaldehyde in the troposphere. *Atm. Environ.* 30/4, 621-638.
- 514 De Heinzelin, J., 1955. Observations sur la g n se de nappe de gravats dans les sols
 515 tropicaux. Publication de l'INEAC, s rie Scientifique, 64, Brussels.
- 516 De Ploey, J., 1964. Stone-lines and clayey-sandy mantles in lower Congo: their formation and
 517 the effect of termites. In: Bouillon, A. (Ed.), *Etudes sur les Termites Africains*, Universit 
 518 de Louvanium, Leopoldville, 399-414.
- 519 Donkin, M. J., Fey, M. V., 1991. Factor analysis of familiar properties of some Natal soils
 520 with potential for afforestation. *Geoderma* 48, 3/4, 297-304.
- 521 Eschenbrenner, V., 1986. Contribution des termites   la microagr gation des sols tropicaux.
 522 *Cah. ORSTOM s r. P dol.* 22, 397-408.

- 523 Eschenbrenner, V., 1987. Les glèbules des sols de Côte d'Ivoire. Thèse faculté Sciences,
 524 Université de Bourgogne, France.
- 525 Eschenbrenner, V., Grandin, G., 1970. La sequence de cuirasses et ses différenciations entre
 526 Agnibilékrou (Côte d'Ivoire) et Diébougou (Haute-Volta). Cah. ORSTOM, sér. Géol. II
 527 (2), 205-245.
- 528 Gleeson, C.F., Poulin, R., 1989. Gold exploration in Niger using soils and termitaria. J.
 529 Geochem. Explor. 31, 253-283.
- 530 Grandin, G., 1976. Aplanissements cuirassés et enrichissement des gisements de manganese
 531 dans quelques regions d'Afrique de l'Ouest. Mém. ORSTOM 82, Paris.
- 532 Humphreys, G. S., 1994. Bioturbation, biofabrics and the biomanatle : an example from the
 533 Sydney basin. In: Ringose-Voase, A.J., Humphreys, G.S. (Eds.), Soil micromorphology :
 534 studies in management and genesis, , Developments in Soil Science 22, 421-436.
- 535 Lebart, L., Morineau, A., Fénélon, J.P., 1979. Traitement des données statistiques.
 536 Dunod, Paris.
- 537 Leprun, J-C, 1979. Les cuirasses ferrugineuses des pays cristallins de l'Afrique
 538 occidentale sèche- Genèse, transformations, dégradation. Mém. Sci. Géol.,
 539 Strasbourg, France.
- 540 Litaor, M. I., Dan, Y., Koyumdjisky, H., 1989. Factor analysis of a lithosequence in the
 541 northeastern Samaria steppe (Israel). Geoderma 44, 1-15.
- 542 Mackenzie, F. T., 1998. Our changing planet. An introduction to earth system science
 543 and global environmental change. Prentice Hall.
- 544 Mando, A., Stroosnijder, L., Brussard, L., 1996. Effects of termites on infiltration into
 545 crusted soil. Geoderma 74, 107-113.
- 546 Mazaltarim, D., 1989. Géochimie des cuirasses ferrugineuses et bauxitiques de l'Afrique de
 547 l'Ouest et Centrale. Ph. D Thesis, University of Strasbourg, France.

- 548 Michel, P., 1973. Les bassins des fleuves Sénégal et Gambie: étude géomorphologique. Mém.
 549 ORSTOM 63, Paris.
- 550 Miedema, R., Brouwer, J., Geiger, S. C., Vandenbeldt, R. J., 1994. Variability in the growth
 551 of *Faidherbia albida* near Niamey, Niger, Africa : micromorphological aspects of termite
 552 activity. In: Ringose-Voase, A.J. Humphreys, G.S. (Eds.), Soil micromorphology : studies
 553 in management and genesis, Developments in Soil Science 22, 411-419.
- 554 Millot, G., 1983. Planation of continents by intertropical weathering and pedogenetic
 555 processes. In lateritisation processes, Melfi, A. J., Carvalho, A., Eds, Proceedings of
 556 the II international Seminar on Lateritisation Processes, Sao Paulo, Brazil, 1982, pp.
 557 53-63.
- 558 Nahon D., 1986. Evolution of iron crust in tropical landscapes. In: S.H. Colemans and
 559 D.P. Dethier (Eds.), Rates of Chemical weathering of rocks and minerals, Chap. 9,
 560 169-191.
- 561 Nahon D., 1991. Introduction of the petrology of soils and chemical weathering. John Wiley
 562 & Sons, New York.
- 563 Nahon D., Melfi A., Conte C. N., 1989. Présence d'un vieux système de cuirasses
 564 ferrugineuses latéritiques en Amazonie du Sud- Sa transformation *in situ* en latosols
 565 sous la forêt équatoriale actuelle. C. R. Acad. Sci., Paris, sér. II, 308, 755-760.
- 566 Novikoff A., 1974. L'altération des roches dans le massif du Chaillu (République
 567 populaire du Congo). Formation et évolution des argiles en zone ferrallitique. Thèse
 568 Sc., University of Strasbourg, France.
- 569 Roquin, C., Freyssinet, Ph., Zeegers, H., Tardy, Y., 1990. Element distribution patterns in
 570 laterites of southern Mali: consequence for geochemical prospecting and mineral explora-
 571 tion. Applied Geochem. 5, 303-315.

- 572 Runge, J., 2002. Holocene landscape history and palaeohydrology evidenced by stable carbon
573 isotope $\delta^{13}\text{C}$ analysis of alluvial sediments in the Mbari valley (5° N/ 23° E), Central
574 African Republic. *Catena* 48/1-2, 67-87.
- 575 Runge, J., Lammers, K., 2001. Bioturbation by termites and late quaternary landscape
576 evolution on the Mbomou plateau of the Central African Republic (CAR). In: van
577 Zinderen Bakker Sr., Heine K. (Eds.), *Palaeoecology of Africa and of the surroundings*
578 *Islands* 27, 153-169.
- 579 Sillans, R., 1958. *Les savanes de l'Afrique Centrale*. Lechevalier, Paris.
- 580 Tardy, Y., 1997. *Petrology of laterites and tropical soils*. Balkema, Amsterdam.
- 581 Tardy Y. and Nahon D., 1985. Geochemistry of laterites, stability of Al-goethite, Al-hematite
582 and Fe^{3+} -kaolinite in bauxites and ferricretes : an approach to the mechanism of concretion
583 formation. *Am. J. Sci.* 285, 865-903.
- 584 Tardy, Y., Mazaltarim, D., Boeglin, J.L., Roquin, C., Pion, J.C., Paquet, H., Millot, G., 1988.
585 *Lithodépendance et homogénéisation de la composition minéralogique et chimique des*
586 *cuirasses ferrugineuses latéritiques*. *C. R. Acad. Sci., Paris, sér. II*, 307, 1715-1722.
- 587 Tardy, Y., Roquin, C., 1992. Geochemistry and evolution of lateritic landscapes. In: Martini,
588 I. P., Chesworth, W. (Eds.), *Weathering, Soils & Paleosols, Developments in Earth*
589 *Surface Processes* 2, 407-471.
- 590 Tardy, Y., Roquin, C., 1998. *Dérive des continents, Paléoclimats et altérations tropicales*.
591 BRGM editions, Orléans, France.
- 592 Thomas, M. F., 1994. *Geomorphology in the tropics. A study of weathering and denudation in*
593 *low latitudes*. John Wiley & Sons.
- 594 Trolard, F., Tardy, Y., 1987. The stabilities of gibbsite, boehmite, aluminous goethites and
595 aluminous hematites in bauxites, ferricretes and laterites as a function of water activity,
596 temperature and particle size. *Geochim. Cosmochim. Acta* 51/4, 945-957.
- 597

Figures caption

Figure 1. (a) Location of the study area in Central African Republic (CAR). The black rectangle represents the previous mapped land area (Beauvais and Roquin, 1996; Beauvais, 1999). (b) Geomorphic distribution of the different forms of ferricrete. The black square is for the location of the disaggregated-ferricrete profile at Guénékoumba. (c) Geomorphological transect across c shown in (b).

Figure 2. (a) Sketch of a typical undisturbed profile, (b) Macroscopic patterns of the disaggregated ferricrete, (c) and (d) disaggregated ferricrete profiles of Guenekoumba and Finzani, respectively. The grey and black squares represent the analyzed samples.

Figure 3. (a) Gently sloping surface (bare hillslope) colonized by termite mounds, (b) Detail of the mounds at the transition between the grassy and forested hillslope (the size of the foreground ferricrete block is 0.5-0.6 m).

Figure 4. Transformation of a red-black hematite-kaolinite nodule into yellow goethite, (a) Polarised optical microscope view, (b) Scanning electron microscope view (Go = goethite crystals developing perpendicular to the nodule edge; kHe = kaolinite-hematite core of the nodule).

Figure 5. Transformation of kaolinite into gibbsite in a nodule, (a) Polarised optical microscope view. (b) Scanning electron microscope view. (K= kaolinite; G= Gibbsite).

Figure 6. Scanning electron micrographs of the bioturbated micro-aggregated clay ferruginous matrix. (a) Microcrystalline newly formed gibbsite, (b) detail of (a), (c) relict quartz grain and (d) relict quartz grain with dissolution-crystallization figures. (kHe = kaolinite-hematite; G = gibbsite; Q = quartz).

Figure 7. Geochemical comparison between undisturbed ferricrete profile (grey) and the disaggregated ferricrete horizon (black) of Guenekoumba, (a) Fe vs. Sc, (b) Fe vs. Zr, (c) Si vs. Zr, and (d) Ti vs. Zr, (the dashed line represents the relative accumulation and/or depletion of chemical elements).

Figure 8. Geochemical differentiation pattern of the components in the undisturbed and disaggregated profiles of Guenekoumba by the factor score diagram Fs1 vs. Fs2, (see the table 1 for the factor loadings, and the figure 7 for the labels explanation). (Af = advancing ferruginization; Fd = ferricrete degradation).

Figure 9. Geochemical differentiation pattern of the degradation components in the disaggregated ferricrete horizons of Guenekoumba (black) and Finzani (grey) by the factor score diagram Fs1 vs. Fs2, (see the table 3 for the factor loadings, and the figure 7 for the labels explanation).

Figure 10. Comparison between each disaggregated ferricrete profile, (a) quartz content vs. ratio RKGi in the degradation matrices ($RKGi = 100 * \text{kaolinite} / \text{kaolinite} + \text{gibbsite}$), (b) Ti vs. Zr (see Figures 7 and 9 for labels explanation).

Figure 11. Comparison between the two disaggregated ferricrete profile (a) kaolinite vs. gibbsite contents, (b) Fe vs. Zr (see Figures 7 and 9 for labels explanation)

649 **Tables caption**

650

651 **Table 1.** Correlation of chemical elements and minerals with each orthogonal
 652 factorial axis defined by the Principal Component Analysis for the undisturbed
 653 and disaggregated ferricrete profiles (σ %= % of explained variance; loading
 654 values are given in parentheses)

655

656 **Table 2.** Mean chemical and mineralogical compositions of the ferricrete
 657 degradation components (N = number of samples; m = mean; $\sqrt{\sigma}$ = standard
 658 deviation; wt.= weight; LOI = lost on ignition (1000°C); RHG= 100 * hematite /
 659 hematite + goethite; RKGi= 100 * kaolinite / kaolinite + gibbsite).

660

661 **Table 3.** Correlation of chemical elements and minerals with each orthogonal
 662 factorial axis defined by the Principal Component Analysis for the two
 663 disaggregated ferricrete profiles (σ %= % of explained variance; loading values
 664 are given in parentheses)

665

666

Figure

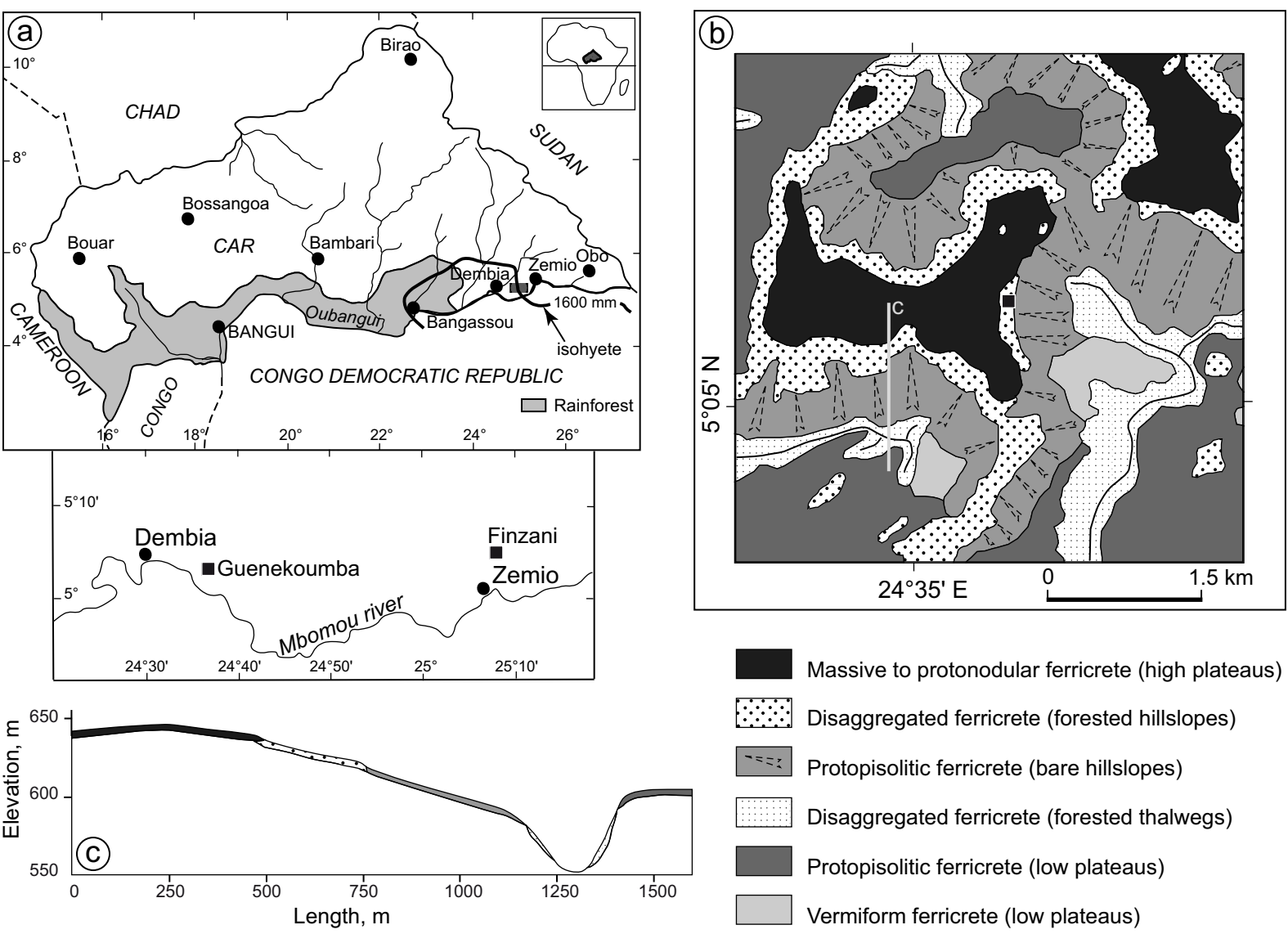


Fig. 1

Beauvais, 2008

Figure

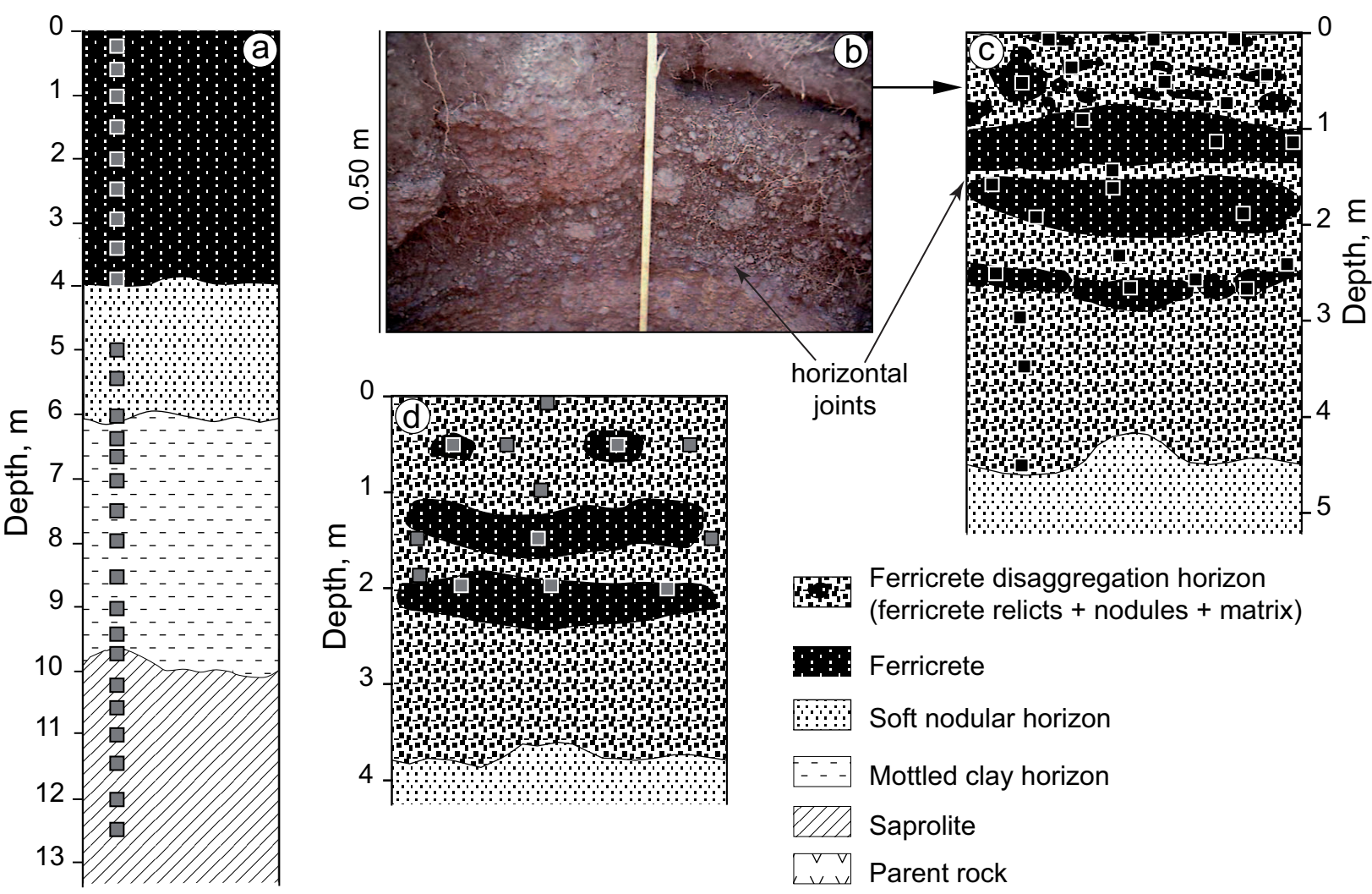


Fig. 2

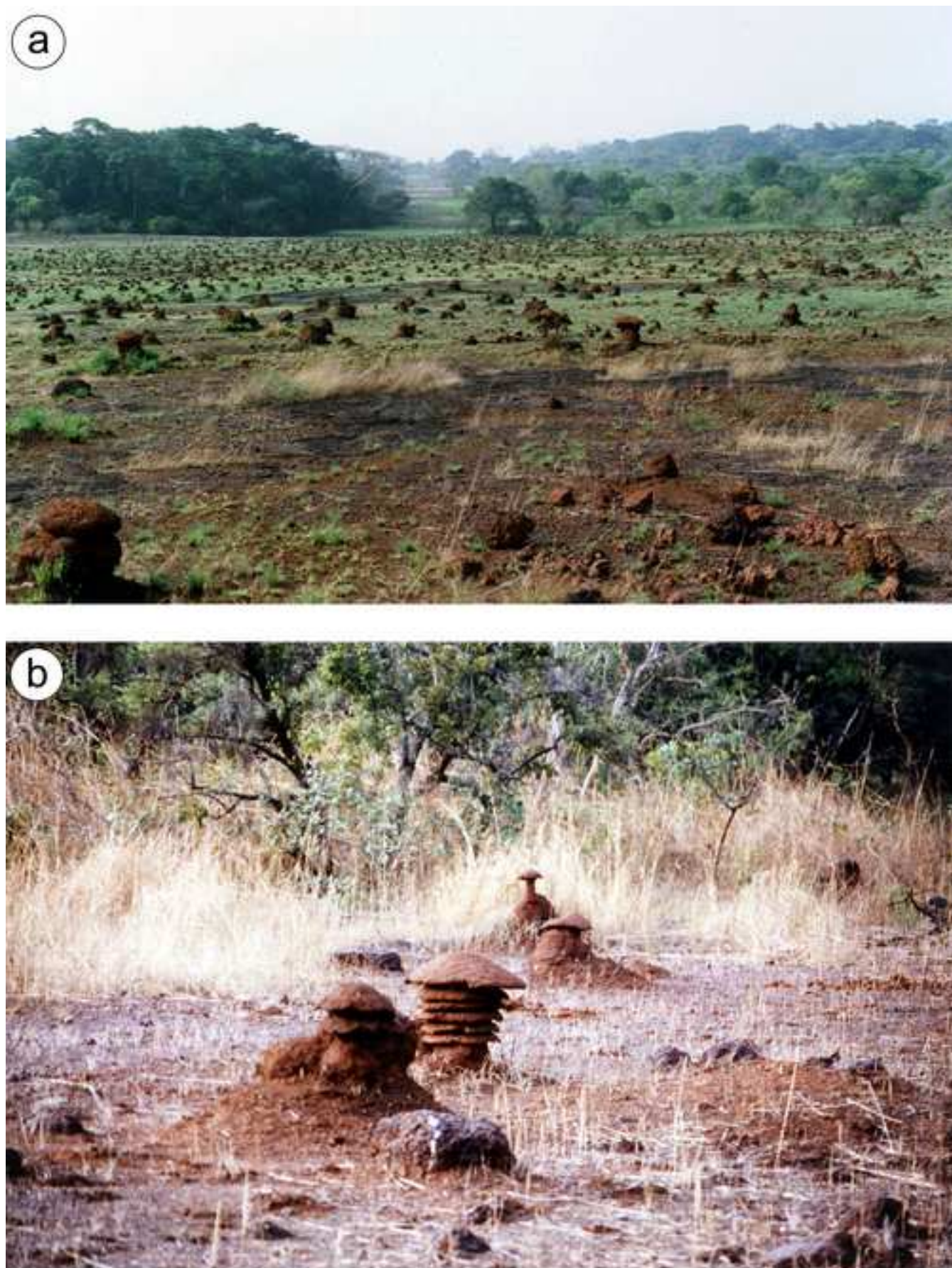


Fig. 3

Beauvais, 2008

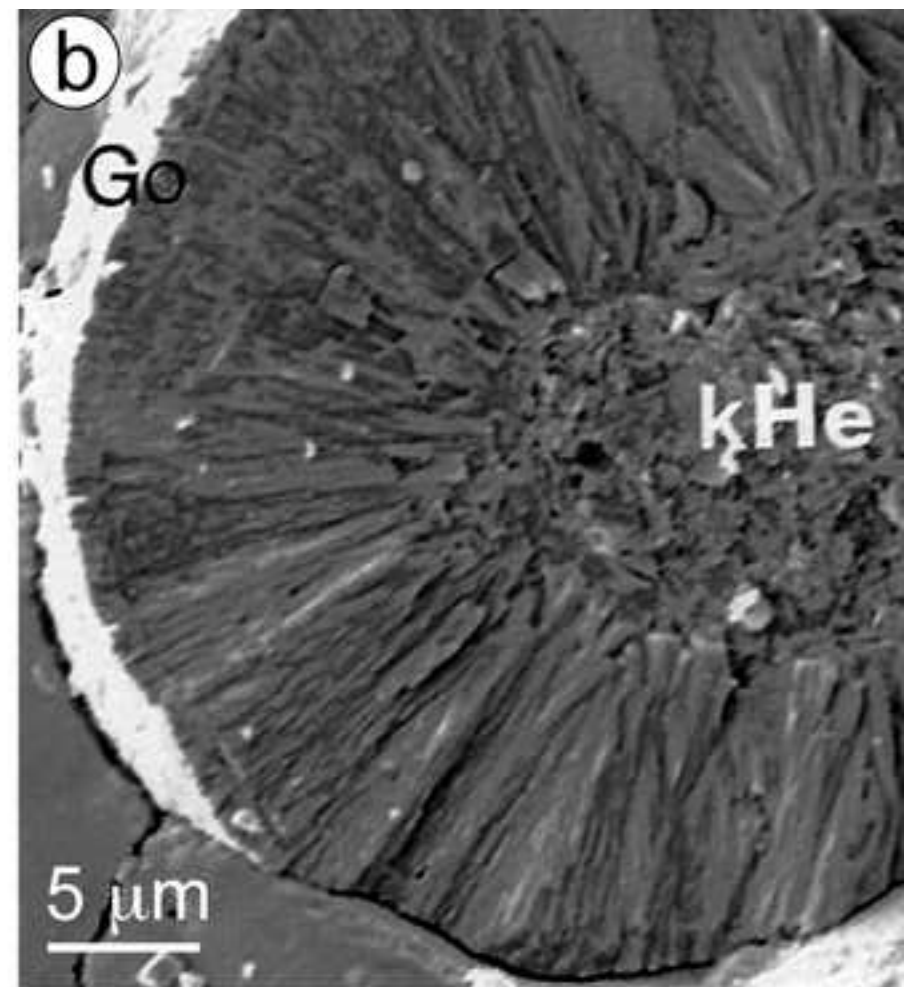
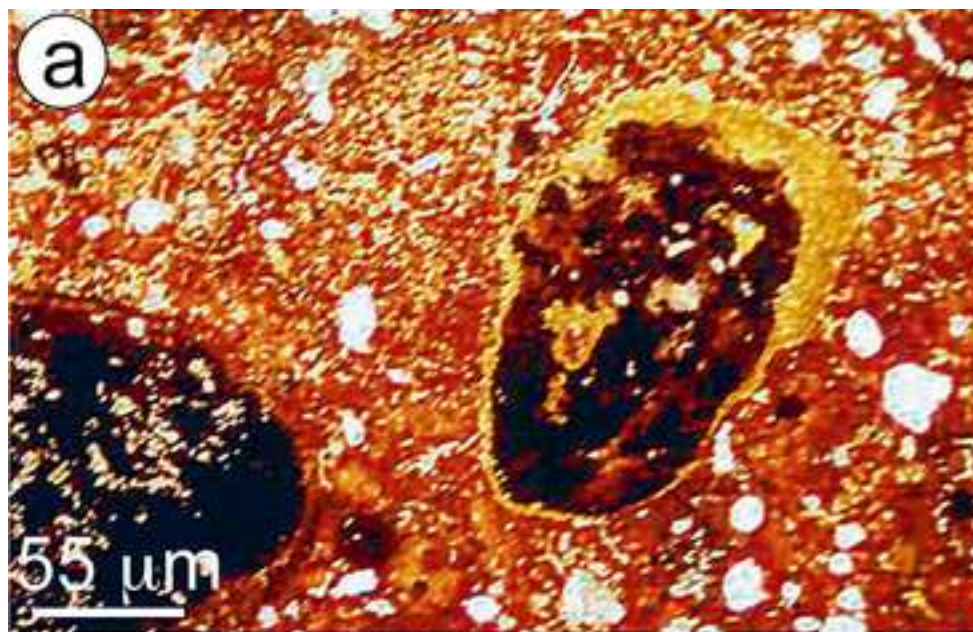


Fig. 4

Beauvais, 2008

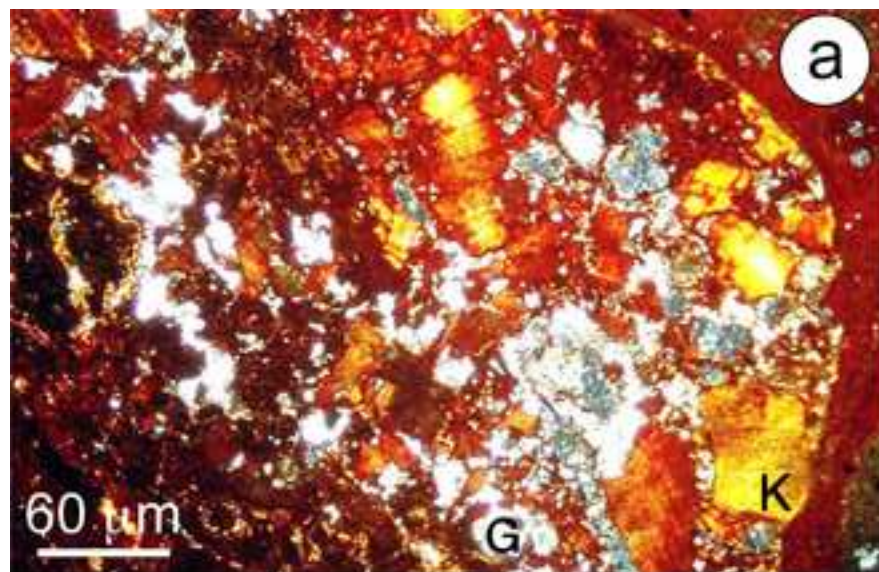
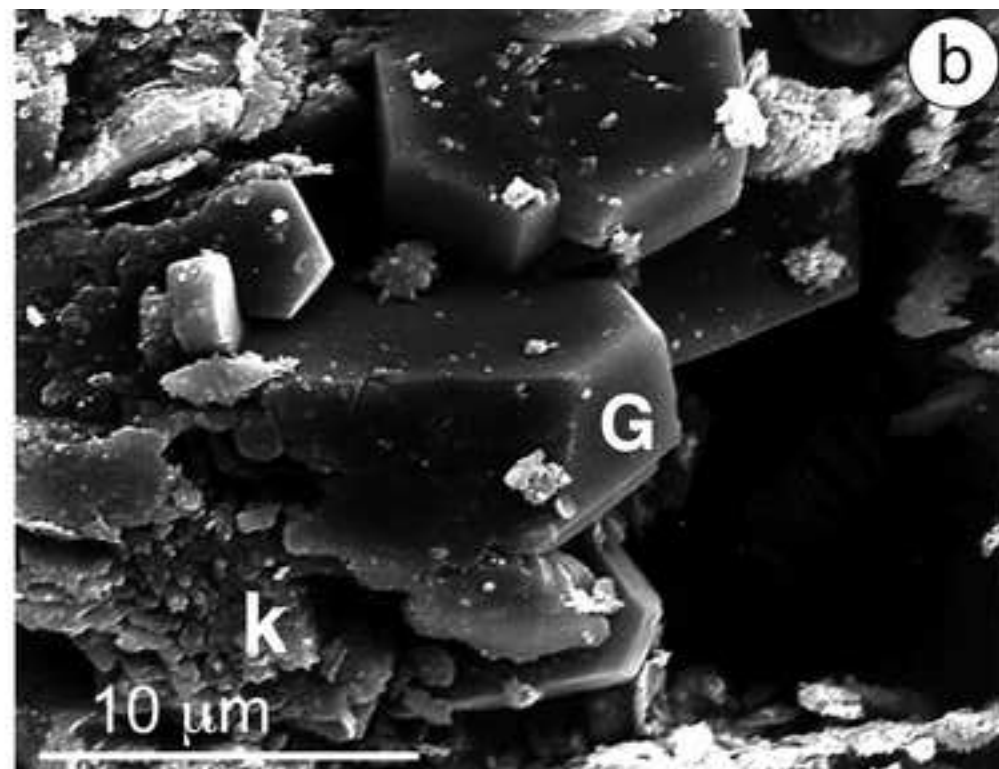


Fig. 5

Beauvais, 2008



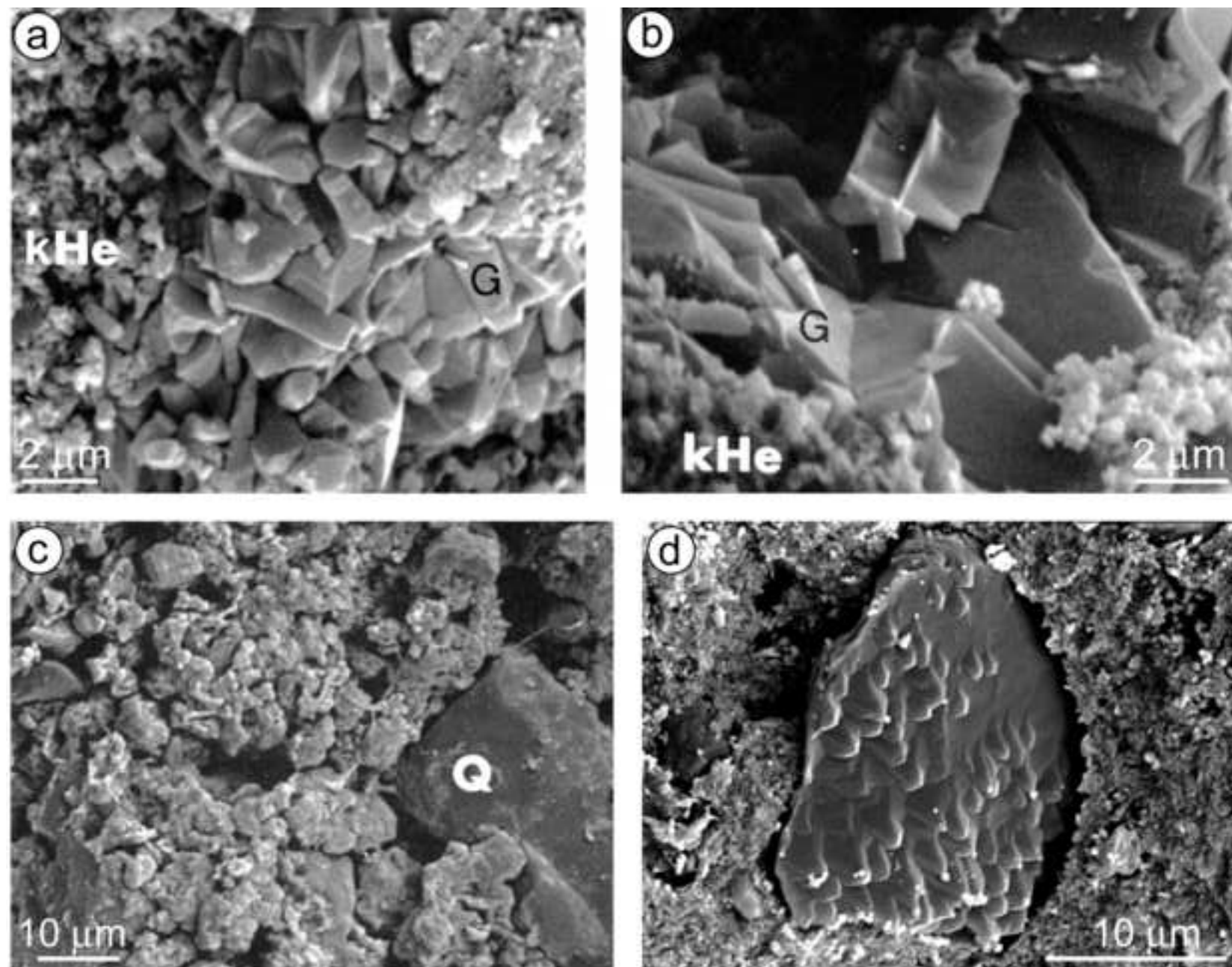


Fig. 6

Beauvais, 2008

Figure

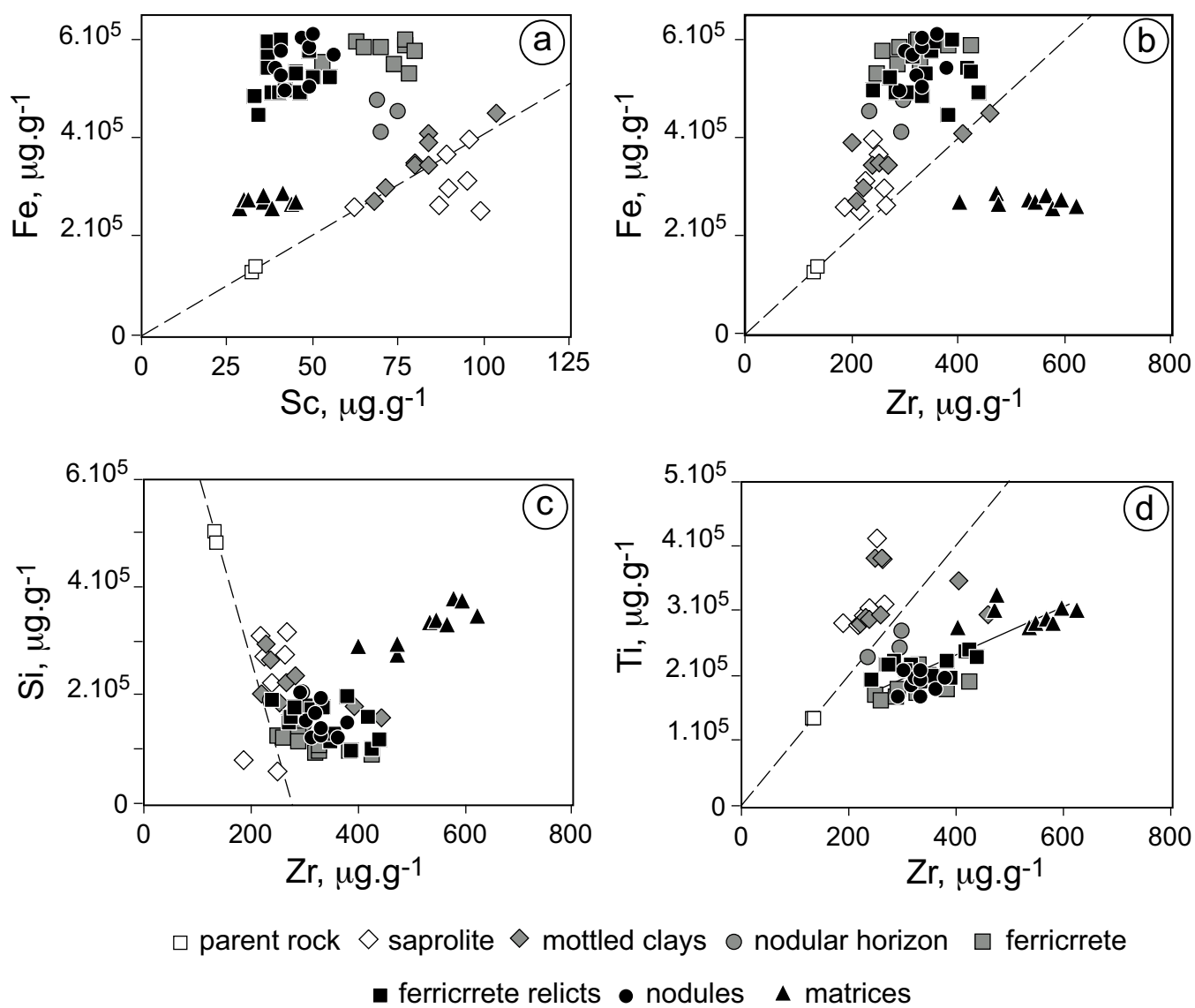


Fig. 7

Figure

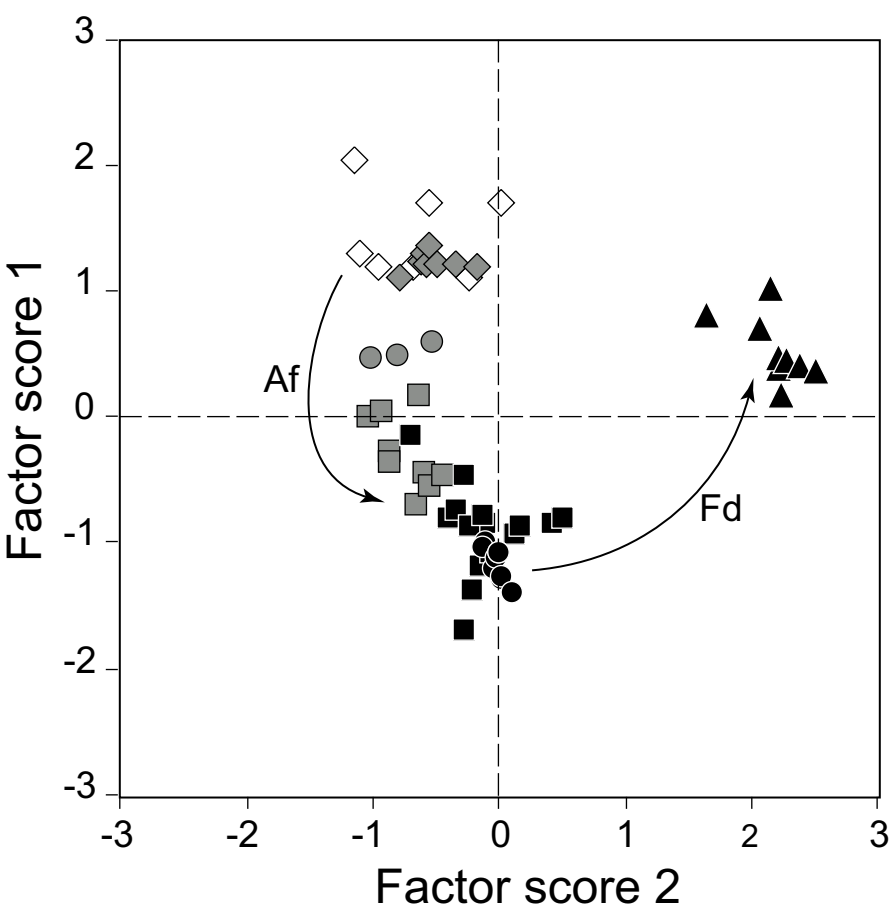


Fig. 8
Beauvais, 2008

Figure

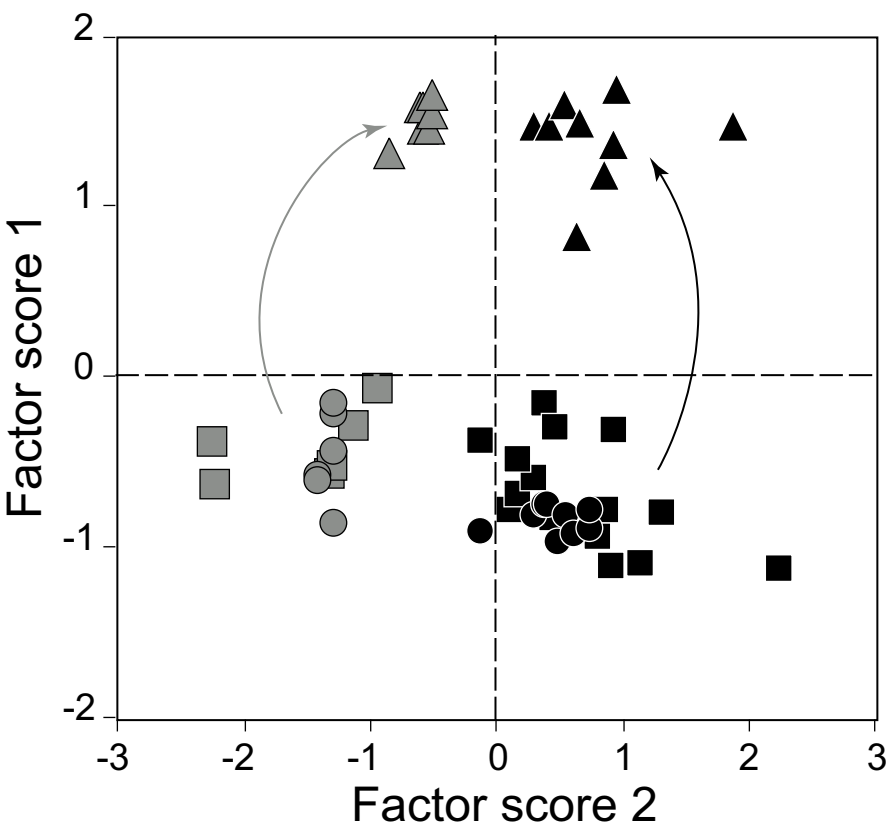


Fig. 9
Beauvais, 2008

Figure

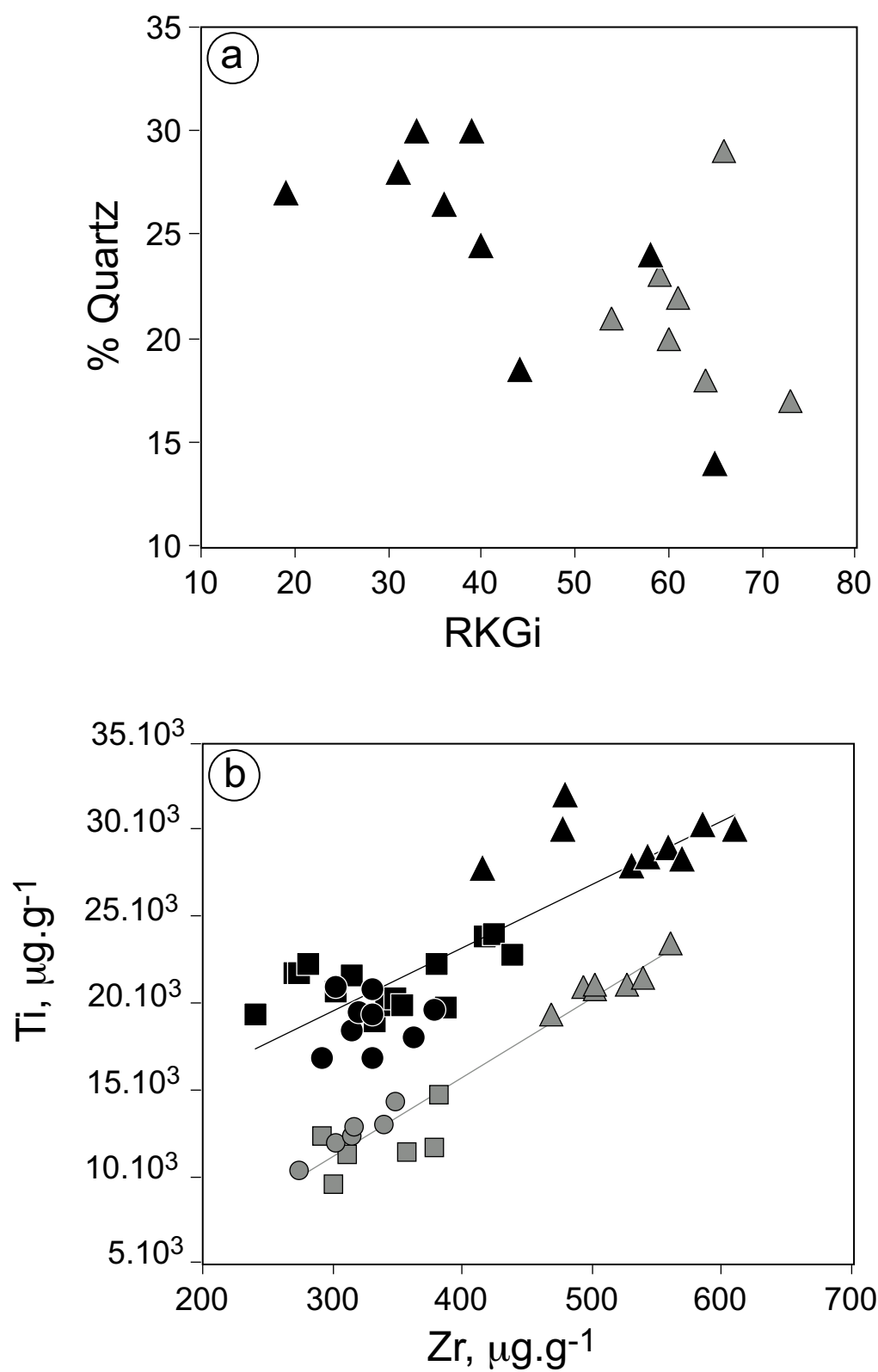


Fig. 10

Beauvais, 2008

Figure

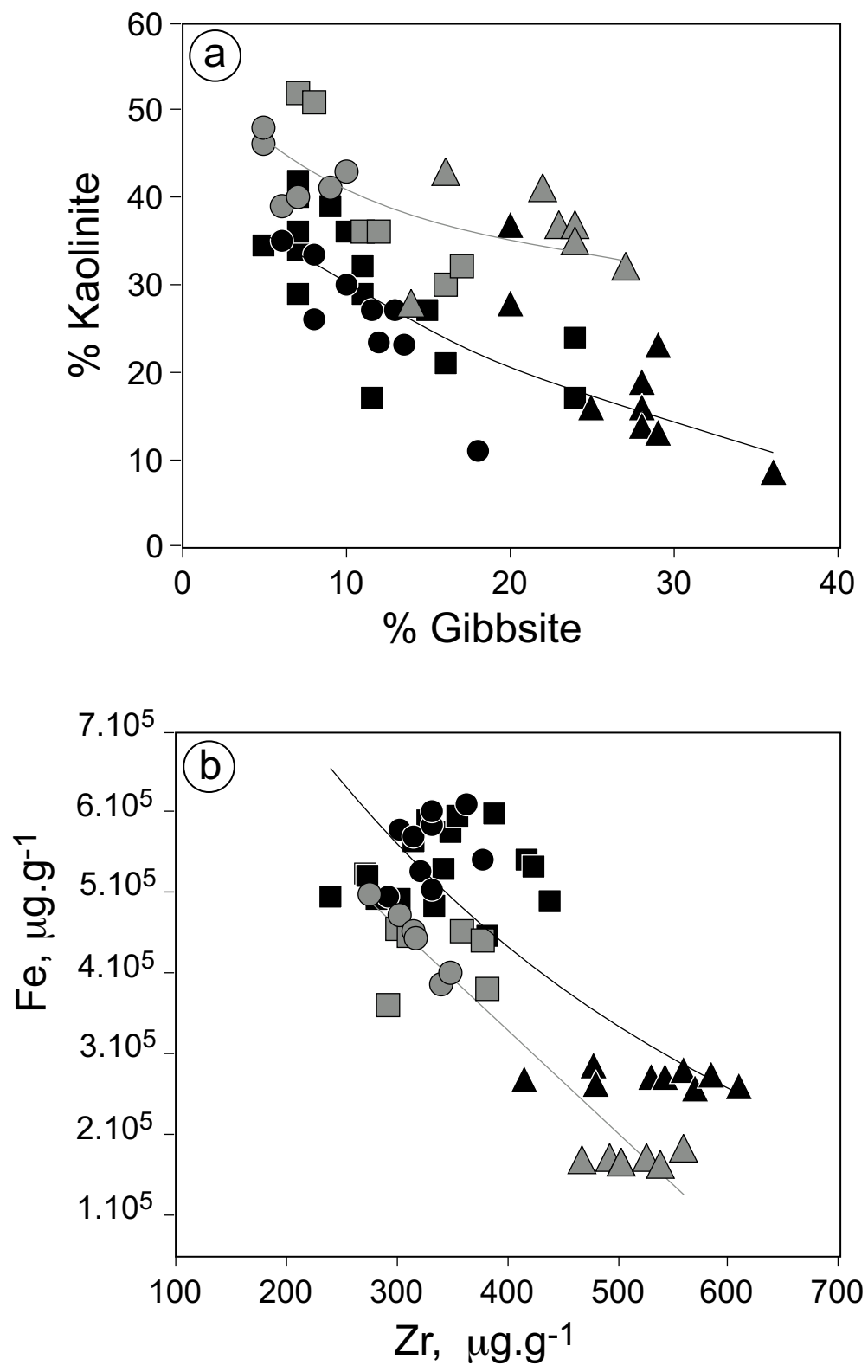


Fig. 11

Factorial Axis	σ %	Positive loading	Negative loading
F1	37.3	Mn ₃ O ₄ (0.87) TiO ₂ (0.81) Al ₂ O ₃ (0.76) Y (0.71) Ni (0.71) Zn (0.71) Sc (0.66) Goethite (0.60) SiO ₂ (0.53) Kaolinite (0.52) Cu (0.50)	Hematite (0.94) Fe ₂ O ₃ (0.81) Cr (0.76) P ₂ O ₅ (0.75) La (0.57) V (0.56) Sr (0.56)
F2	23.6	Quartz (0.93) Nb (0.89) Zr (0.87) MgO (0.73) Yb (0.71) SiO ₂ (0.63) Gibbsite (0.52) Y (0.52)	V (0.66) Sc (0.65) Goethite (0.57) Cu (0.53) Fe ₂ O ₃ (0.48) Kaolinite (0.43)
F3	7.2	Gibbsite (0.76)	Kaolinite (0.66) SiO ₂ (0.47)
F4	7.1	Ce (0.80) Ba (0.77) Sr (0.76) La (0.69)	

Table 1.

Location:	Guenekoumba profile						Finzani profile					
Facies:	Ferricrete		Nodules		Matrices		Ferricrete		Nodules		Matrices	
N:	15		9		9		6		6		7	
	m	√σ	m	√σ	m	√σ	m	√σ	m	√σ	m	√σ
SiO ₂ wt.%	14.89	3.35	15.17	3.11	32.83	3.15	21.73	3.94	22.75	2.4	37.87	1.52
Al ₂ O ₃	19.21	2.44	17.27	1.15	24.53	1.62	23.47	1.63	21.93	2.2	29.67	1.15
Fe ₂ O ₃	52.55	4.38	55.6	4.16	27.03	0.91	42.27	4.06	44.2	4.2	17.03	0.67
Mn ₃ O ₄	0.06	0.02	0.04	0.01	0.09	0.02	0.02	0.01	0.03	0	0.05	0.02
MgO	0.03	0.01	0.04	0.01	0.17	0.07	0.23	0.14	0.22	0.02	0.37	0.02
K ₂ O					0.11	0.02	0.61	0.55	0.46	0.06	0.35	0.08
TiO ₂	2.12	0.15	1.89	0.15	2.93	0.14	1.18	0.17	1.25	0.12	2.12	0.12
P ₂ O ₅	0.39	0.06	0.38	0.05	0.25	0.04	0.19	0.03	0.19	0.01	0.18	0.02
LOI	10.11	1.39	9.27	0.95	11.63	1.45	10.65	0.99	9.11	1.02	12.85	0.35
Sr ppm	39	32	48	9	18	5	34	20	35	7	21	2
Ba	32	24	51	14	40	7	223	179	157	19	95	12
V	1369	280	1298	66	634	29	827	202	757	69	344	14
Ni	47	19	36	6	78	23	35	10	51	6	79	21
Co	13	5	11	2	13	4	9	8	16	3	20	4
Cr	340	142	426	117	155	20	403	157	414	79	91	1
Zn	52	19	50	5	62	16	34	14	40	8	40	8
Cu	133	64	121	19	116	29	58	9	75	5	89	5
Sc	42	6	46	6	37	5	36	3	37	1	40	2
Y	8	2	8	1	23	2	12	2	12	3	31	2
Zr	341	60	329	27	530	61	337	40	316	26	513	31
La	47	39	51	12	23	5	34	12	39	6	33	5
Ce	114	80	99	27	126	20	62	33	65	18	107	11
Yb	1	0	1	0	3	0	2	0	2	0.5	4	0
Nb	18	4	19	2	36	3	16	2	14	3	33	4
% Quartz	1	1	3	3	25	5	3	2	3	1	22	4
Kaolinite	31	8	27	7	19	9	40	10	44	3	38	5
Hematite	41	6	45	5	17	1	33	6	37	4	9	1
Goethite	16	6	14	3	12	1	12	3	8	1	9	1
Gibbsite	11	6	11	4	27	5	12	4	8	2	22	5
RHG	72	10	76	6	57	4	73	8	82	3	52	3
RKGi	72	14	71	14	41	14	76	10	86	4	63	6

Table 2.

Factorial Axis	σ %	Positive loading	Negative loading
F1	44.1	Y (0.95) Yb (0.95) Quartz (0.94) SiO ₂ (0.92) Zr (0.91) Nb (0.90) Al ₂ O ₃ (0.82) Gibbsite (0.78) Ni (0.66) MgO (0.62) TiO ₂ (0.59) Mn ₃ O ₄ (0.40)	Fe ₂ O ₃ (0.94) Hematite (0.91) V (0.78) Cr (0.74) P ₂ O ₅ (0.57) Sr (0.40)
F2	20.9	Cu (0.75) TiO ₂ (0.75) Zn (0.71) P ₂ O ₅ (0.69) Mn ₃ O ₄ (0.67) Goethite (0.63) Sc (0.48)	K ₂ O (0.79) Ba (0.77) kaolinite (0.65) MgO (0.60)
F3	11.4	Co (0.59) Cu (0.52) Sc (0.40) Ni (0.40)	Ce (0.78) La (0.75) Sr (0.75) V (0.42)

Table 3.